

Raman spectroscopy on transition metals

Bin Ren · Guo-Kun Liu · Xiao-Bing Lian ·
Zhi-Lin Yang · Zhong-Qun Tian

Received: 10 October 2006 / Revised: 17 January 2007 / Accepted: 19 January 2007 / Published online: 21 February 2007
© Springer-Verlag 2007

Abstract Surface-enhanced Raman spectroscopy (SERS) has developed into one of the most important tools in analytical and surface sciences since its discovery in the mid-1970s. Recent work on the SERS of transition metals concluded that transition metals, other than Cu, Ag, and Au, can also generate surface enhancement as high as 4 orders of magnitude. The present article gives an overview of recent progresses in the field of Raman spectroscopy on transition metals, including experimental, theory, and applications. Experimental considerations of how to optimize the experimental conditions and calculate the surface enhancement factor are discussed first, followed by a very brief introduction of preparation of SERS-active transition metal substrates, including massive transition metal surfaces, aluminum-supported transition metal electrodes, and pure transition metal nanoparticle assembled electrodes. The advantages of using SERS in investigating surface bonding and reaction are illustrated for the adsorption and

reaction of benzene on Pt and Rh electrodes. The electromagnetic enhancement, mainly lightning-rod effect, plays an essential role in the SERS of transition metals, and that the charge-transfer effect is also operative in some specific metal–molecule systems. An outlook for the field of Raman spectroscopy of transition metals is given in the last section, including the preparation of well-ordered or well-defined nanostructures, and core-shell nanoparticles for investigating species with extremely weak SERS signals, as well as some new emerging techniques, including tip-enhanced Raman spectroscopy and an in situ measuring technique.

Keywords Interface/surface analysis · Raman spectroscopy · Nanoparticles/nanotechnology · Hydrocarbons · Kinetics · Metals

Introduction

Since the observation and discovery of surface-enhanced Raman phenomenon of adsorbed species on roughened Ag surfaces in the mid-1970s [1–3], surface-enhanced Raman spectroscopy has received wide application in fields including surface sciences, electrochemistry, analytical chemistry, biological and biomedical sciences, and forensic science [4–14]. Two mechanisms have been widely accepted to account for the SERS effect observed on coinage-metal surfaces (Ag, Au, and Cu), the electromagnetic (EM) and the charge-transfer (CT) mechanisms [15–18]. The EM effect is the major contribution to the observed SERS signal and has a long-range character, which is considered to predominately arise from surface plasmon resonances together with the contribution of a

B. Ren (✉) · G.-K. Liu · X.-B. Lian · Z.-Q. Tian
State Key Laboratory for Physical Chemistry of Solid Surfaces
and Department of Chemistry,
College of Chemistry and Chemical Engineering,
Xiamen University,
Xiamen 361005, China
e-mail: bren@xmu.edu.cn

Z.-L. Yang
Department of Physics, Xiamen University,
Xiamen 361005, China

Present address:
G.-K. Liu
State Key Laboratory of Chemo/Biosensing and Chemometrics,
Hunan University,
Changsha 410082, China

lightning-rod effect when high surface curvature or sharp edges exist [15, 16]. The CT effect, mainly arising from a photo-driven charge-transfer process, has also been found in numerous experiments to change the SERS signal signatures of specific systems and is a short-range effect [17, 18]. Of the 6 orders of magnitude of total SERS enhancement of an ensemble system, the contribution of CT may account for up to 1 to 2 orders of magnitude [8].

Shortly after the discovery of the SERS effect, it was found that the giant enhancement for practical application is limited to the three coinage metals Ag, Au, and Cu with free electrons, on which the surface plasmon resonances can be easily excited in the visible to the near-infrared light region [15–19]. Other important transition metals in surface sciences are generally not considered SERS-active, because of the difficulty of exciting the surface plasmon resonances in the visible light region. This limits the application of SERS to a great extent.

In order to extend SERS to other transition metal substrates, a strategy based on “borrowing SERS” was proposed in the 1980s, either by depositing SERS-active metals onto non-SERS-active substrates [20, 21] or by depositing non-SERS-active materials over SERS-active substrates [22–26]. The latter strategy receives wide application for studying the surface processes on transition metal overlayers. For example, SERS-active Ag or Au electrodes were coated with ultrathin films of other metals, such as Ni, Co, Fe, Pt, Pd, Rh, and Ru, by electrodeposition. With the aid of the long-range effect of the EM enhancement created by the SERS-active substrate underneath, weak SERS spectra of adsorbates on the transition metal overlayers have been obtained [22–26]. Due to the damping of the strong electromagnetic field under the existence of overlayer films, the film has to be ultrathin, which makes it very difficult to completely cover the rough substrates with such a thin film. Thus, a “pinhole” in the overlayer made it extremely difficult to eliminate entirely the giant contribution of the SERS of the substrate [12]. This problem was overcome partially by Weaver et al. in the mid-1990s. They reported a series of work on preparing pinhole-free transition metal films over the SERS-active Au surface by using constant-current deposition at a low current density [27–29] or by redox replacement of underpotential-deposited metals on Au [30], which allows them to obtain a wealth of information under in situ electrochemical or catalytic reaction conditions. In addition to studying surface adsorption and reaction, the overlayer method has been used to characterize the fine structure of the ultrathin film itself, including surface oxides and semiconductors [31]. The essence of this method is to employ the huge enhancement provided by the highly SERS-active Ag or Au substrate regardless of whether the other transition metals themselves are SERS-active.

Another conceptually different strategy is to use the SERS of transition metals, i.e., transition metals themselves are SERS-active. This strategy is much more challenging as it contradicts to the commonly accepted notion that transition metals are not SERS-active. Several groups attempted to obtain surface Raman signals from adsorbates on either roughened or mechanically polished Pt and Rh electrodes, or porous Ni, Pd, Pt, Ti, and Co films [32–42]. However, the reported surface Raman spectra could be obtained only under optimal conditions or by data manipulation using spectral subtraction methods and the surface Raman signals were typically too weak to be investigated as a function of the electrode potential or temperature although this is essential for practical applications. Indeed, only a few papers, among many theoretical and experimental works, claimed that transition metals might have relatively weak SERS activity in comparison with the coinage metals of Au, Ag, and Cu [19, 38–42]. However, these were not fully accepted by the scientific community.

The situation has changed dramatically since the late-1990s. The single-grating confocal Raman instruments equipped with notch filters or edge filters now provide unprecedented sensitivity and can effectively eliminate the interference of the signal of the bulk phase. This is very helpful for obtaining the very weak signal of the surface species. Our group has benefitted from this advancement in Raman instruments and we have made further efforts to optimize the experimental setup as well as to properly treat the transition metal surfaces [12, 13, 43]. Thereby, we have been able to obtain good-quality surface Raman signals from bare Pt, Ru, Rh, Pd, Fe, Co, and Ni electrodes of a large variety of molecules, including model molecules and molecules with practical application [44–49]. We found that transition metals exhibit surface enhancement factors ranging from 1 to 4 orders of magnitude, depending on the nature of metal and the surface morphology.

In the meantime, the rapid development of nanotechnology has provided new opportunities for the SERS of transition metal systems. Li and Yang group reported the SERS from Fe nanoparticles surfaces [50]. Gómez et al. employed a microemulsions method to fabricate spherical Pt-group nanoparticles with an average diameter of 4 nm and obtained an enhancement of ca. 550 for Pt [51–53]. Xia's group synthesized Pd nanoparticles with controlled size and shape, and obtained a maximum enhancement of 4 orders of magnitude for Pd [54–56]. By using a laser ablation method, Kim's group was able to fabricate Pt nanoparticles with a size about 17 nm and obtained an enhancement of ca. 2 orders of magnitude [57, 58].

SERS studies on massive transition metal electrodes and transition metal nanoparticles show that transition metals themselves are SERS-active and the surface enhancement depends very much on the nature of the metal, the surface

pretreatment, and the shape and size of nanoparticles [38–58]. That Pd nanobox can provide an enhancement of 4 orders of magnitude points to the bright future of the SERS of transition metals [56]: if one can controllably roughen the surface to achieve an ideal surface structure or synthesize nanoparticles with suitable shape and size, it will be possible to achieve the necessary enhancement effect for practical applications.

Experimental considerations

It should be emphasized that although some transition metals are SERS-active, the enhancement is still weaker than that of coinage metals [1–18, 43–58]. To extract the very weak signal, it is important to optimize the experimental setup to extract information that may have been overwhelmed by the background signal. In a confocal Raman microscope, the objective plays a key role as it introduces the laser and collects the Raman signal. Under electrochemical conditions, in between the objective and the surface, there is an optical window and electrolyte whose refractive indices are different from the designed value of the objective to be used in air. Therefore, the laser spot that should have been tightly focused in air becomes slightly defocused, which prevents the Raman signal of the surface species from passing through the pinhole to the detector. Therefore, the Raman intensity will be significantly decreased. Without careful consideration of the design of the spectroelectrochemical cell, the advantage of the confocal microscope may be lost and the surface Raman signal may not even be detected. For example, a solution layer of large refractive index could affect dramatically the collection efficiency of the microscope by decreasing the solid angle of the system. With an increase in the thickness of the solution layer from about 0.2, 0.5, or 1 mm to 2 mm, the Raman signal intensity remains at 89%, 71%, 52%, and 35%, respectively, of the maximum intensity in air, see Fig. 1 [59]. A thickness of 0.2 mm appears to be optimum for the electrochemical system. Furthermore, in the electrochemical system, most of the electrolytes are corrosive, so that in order to protect the objective, a cover glass or quartz window has to be employed between the electrolyte and the objective. This approach results in a 50% loss of the signal due to the lowering of the laser power density on electrode surface as a result of the defocusing effect of the laser spot. An alternative and the best way, we found, to protect the objective is to wrap it with a very thin and highly transparent poly(vinyl chloride) or polyethylene film. With this approach, the Raman signal only suffers a 10% loss. Hence, optimization of the optical configuration is essentially important in order to realize the full potential of confocal Raman microscopy.

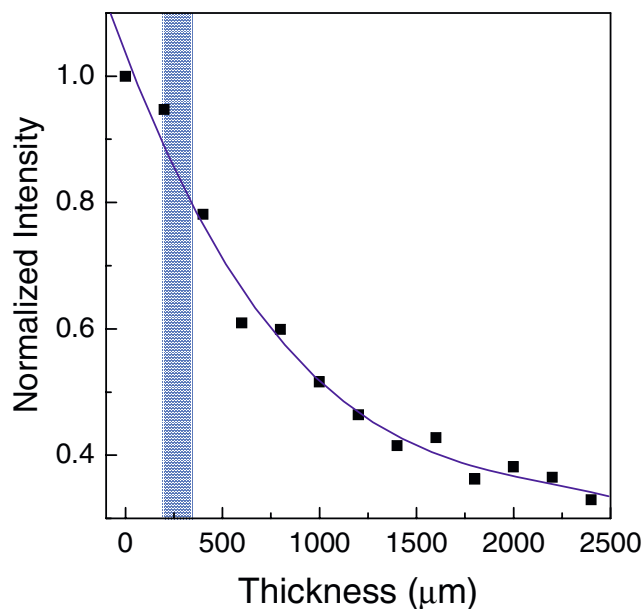


Fig. 1 Effect of the thickness of solution layer between the microscope objective and the silicon wafer on the Raman intensity of the 520.6 cm^{-1} band of Si. The diameter of pinhole is $600\text{ }\mu\text{m}$. The shaded area indicates the ideal thickness for in situ electrochemical study

Preparation of SERS-active transition metal surfaces

Besides the optimization of the experimental setup, a surface with a very high SERS activity is crucially important to the SERS of transition metals. As in the case of coinage metals, the SERS activity of transition metals also depends very much on the morphology of the surface or the size and shape of nanoparticles [12, 13, 38–58]. In the following section, we will briefly introduce the methods that have been used successfully to obtain the SERS from transition metals. The overlayer strategy has been reviewed in great detail by Weaver et al. in 2000 [29] and consequently will not be introduced here.

Electrochemical roughening method

The simplest way to obtain SERS-active transition metal surfaces is to employ an electrochemical roughening method, which can be realized by simply applying an electric control, such as current or potential, on the electrode in a suitable electrolyte. The variables that can be adjusted in the electrochemical roughening method include the oxidation and reduction potentials, the type of potential–time function (e.g., triangular-wave potential sweep or double potential steps), the amount of charge passed for each oxidation step or sweep, the number of cycles, and the composition of electrolyte. The electrochemical method is also generally called oxidation and reduction cycle(s) (ORC). Due to the different electrochem-

ical behavior of different transition metals, it is natural that one should develop different ORC procedures for different metals. In our previous feature article, we have given a list of the roughening methods for transition metals [12]; readers may refer to the paper for the roughening recipe. In the last several years, we have further obtained SERS signals from Pd surfaces [49] and made further improvements on the roughening method of Ni [60]. Therefore, it is necessary to update the roughening recipe in order to improve the enhancement effect in transition metal systems. For the Pd electrode, the roughening solution is 1 M H_2SO_4 . Before roughening, the Pd electrode should first be electrochemically cleaned by potential cycling between -0.2 and 1.2 V at a rate of 0.5 V s^{-1} for about 1 to 2 min. Then, a square-wave potential was applied to the Pd electrode for ca. 20 to 30 s, with an oxidation potential of 1.7 V, a reduction potential of -0.4 V, and a frequency of 600 Hz. Afterwards, the electrode was held at -0.1 V for about 350 s for a complete reduction of the surface oxides formed. For the Ni electrode, the electrode was first ultrasonically cleaned and etched in 0.5 M H_2SO_4 for 30 s to remove surface impurities and oxides. Then, the electrode was kept at -1.3 V for 15 s to allow for severe hydrogen evolution in 0.5 M NaClO_4 to completely remove surface oxides. Afterwards, a square waveform with a frequency of 500 Hz was applied to the electrode for 250 s with an upper potential and lower potential of 0.65 and -1.3 V, respectively. Finally the electrode was kept at -1.1 V for 600 s for a complete reduction of the electrode. It should be noted that, usually before and after the roughening, the electrode should be subjected to electrochemical cleaning or stabilizing in order to remove some unusually chemically active or SERS-active sites to improve the reproducibility.

We have found from 10 years of experience working on SERS of transition metals that in order to obtain a reproducible SERS substrate, it is vitally important to pay attention to the purity of metal, the method of drawing the metal, and the batch of metals. All these parameters influence the crystallinity of the metal surfaces and lead to the existence of crystalline domains of different size and properties. Inevitably, the surface cannot be ideally uniform. Therefore, even under the same conditions, the method may work differently for different batches of metals. However, it is only necessary to make slight modification on the parameters given above.

Chemical etching methods

Besides the SERS-active massive transition metal surfaces, we have also developed different chemical etching methods for obtaining Fe, Co, and Ni surfaces with 1 M H_2SO_4 or 1 M HNO_3 in an ultrasonic bath. This kind of surface

provides moderate surface enhancement. Further electrochemical ORC based on such substrates will slightly boost the enhancement [12].

Another type of chemical etching method is called the chemical replacement approach [61]. By immersing a piece of aluminum that has been polished and pre-cleaned in 0.5 M NaOH solution in an aqueous solution of the metal salt (with concentrations between 0.1 and 1.5 M), aluminum-supported SERS-active transition metal substrates have been obtained [61], which provided huge enhanced Raman signals of pyridine on Ni, Cd, Fe, Ag, Au, and Cu. Although the authors did not calculate the enhancement factor, the strong SERS signal from Fe as compared with Au is really impressive. One should especially note the possible influence of the signal from aluminum on that of the overlaid metals.

Preparation of pure transition metal nanoparticle electrodes

Although it is comparably easy to obtain SERS-active substrates from various transition metal surfaces, the surface structures of electrochemically roughened electrodes are far from controllable considering size, shape, and aggregation states. In comparison, metal nanoparticles of different material and of controllable size, shape, and structure have been routinely synthesized with the rapid development of nanotechnology [51–62]. Furthermore, it has been found that Pt-group nanoparticles have a higher SERS activity than that of massive Pt-group metals, especially in the case of Pt nanospheres and Pd nanoboxes [54, 56]. Therefore, it is worthwhile to introduce the preparation method of some typical systems. For example, 4-nm Pt and Pd nanoparticles have been prepared via water-in-oil microemulsions [51–53]. Then, a certain amount of aqueous solution containing nanoparticles was dispersed over HOPG or Pt surfaces. The electrode was then dried in an Ar flow. Before use for Raman measurement, the electrode was cleaned by hydrogen evolution or CO adsorption and oxidation. Such electrodes can generally present an enhancement factor up to 550 for Pt, which is slightly higher compared with that of the massive electrodes.

The second and more convenient and clean way to prepare nanoparticles is to use a laser ablation method [57, 58]. Pt nanoparticles have been obtained via laser ablation of a Pt plate in triply distilled water for about 60 min using a pulse Nd:YAG laser (1,064 nm). After being centrifuged for at least 5 times at 3,000 rpm for 2 min to remove tiny particles smaller than 2 nm, the resulting sol containing Pt nanoparticles of size ca. 8 nm. The substrate prepared from such nanoparticles can produce surface enhancement up to ca. 100 to 200 for benzenethiole, a non-resonant molecule, similar to that of massive electrodes. As raw materials used in this method are distilled water and high-purity platinum,

the resulting nanoparticles are very clean. However, it should be noted that the size distribution of Pt nanoparticles is relatively broad.

The electromagnetic enhancement mechanism indicates that nanoparticles with sharp edges may produce higher enhancement than spherical nanoparticles [15, 16]. Indeed, Xia's group clearly showed such an effect with their peculiar-shaped nanoparticles, including the nanobox, nanocage, and nanocube [54–56]. Pd nanocubes were synthesized by reducing Na_2PdCl_4 with ethylene glycol in the presence of poly(vinyl pyrrolidone). The size of the cubes could be controlled by adjusting the density of seeds formed in the nucleation step. The synthesis of nanoboxes and nanocages was similar, except water was added to increase the solubility of oxygen and thus oxidative corrosion. A different enhancement effect was found for nanoparticles with different shapes, with maximum enhancement of 1.3×10^4 for the adsorbed *para*-aminothiophenol (PATP) molecules occurring on nanobox [56], which is about 1 order of magnitude higher than that on a massive Pd electrode using pyridine as the probe molecule [49]. Although the existence of a charge-transfer contribution in the present system is still not conclusive, such a high enhancement is very exciting.

We have found that it is extremely difficult to obtain SERS directly in metal colloid solutions, which may be due to the intrinsic weak SERS in the transition metal systems and the lack of a sufficient number of nanoparticle aggregates for effective coupling among nanoparticles as in the case of coinage metals. Instead, most of the SERS investigations of transition metal systems were performed by dispersing metal nanoparticles with known concentration over a substrate that can be metal, glassy carbon, ITO, semiconductors, or even glass slides via natural, inert gas flow or vacuum drying [50–58]. We have found recently that the coupling between not only nanoparticles but also the nanoparticles and the substrate is important to the SERS effect [62, 63]. Usually, the SERS signal from Pt nanoparticles dispersed on Pt electrodes is stronger than that dispersed on glass or glassy carbon surfaces.

With their high enhancement, nanoparticle assembled electrodes are very useful to study adsorption and reaction under mild reaction conditions. However, under vigorous reaction conditions, the nanoparticles can be easily detached from the surfaces. Further attention should be paid to the possible small size effect on the surface chemistry of nanoparticles compared with that of bulk electrodes.

Estimation of surface roughness factor

The calculation of the surface enhancement factor (G) is important when one is going to evaluate the activity of a

new type of SERS substrate. We have proposed in our previous articles a method to calculate the surface enhancement factor of transition metals, based on the confocal configuration [12, 43, 64]. This method has been adopted by many other groups using the confocal Raman instrument. However, we found that this method has been erroneously used in some papers, which led to incorrect estimations of G . Therefore, it is worthwhile to introduce again the calculation method here with emphasis on how to obtain correct experimental data.

Surface enhancement factor (G) can be calculated by:

$$G = \frac{I_{\text{surf}}/N_{\text{surf}}}{I_{\text{bulk}}/N_{\text{bulk}}} \quad (1)$$

where I_{surf} and I_{bulk} denote the integrated intensities for the strongest band of the surface and solution species, respectively, and N_{surf} and N_{bulk} represent the number of the corresponding surface and solution molecules effectively excited by a laser beam. N_{surf} can be calculated by the following approximation, after considering the contribution of the surface roughness:

$$N_{\text{surf}} = \frac{RA}{\sigma} \quad (2)$$

where R is the roughness factor of an electrode, A is the area of the focal spot of the laser; σ is the surface area occupied by an adsorbed molecule. N_{surf} can also be estimated by limiting the number of molecules to slightly less than a monolayer during adsorption. However, the calculation of N_{bulk} is complicated and should be considered very carefully in a confocal Raman microscope. Figure 2a shows the waist profile of a focused laser beam in an aqueous solution. In principle, all molecules within

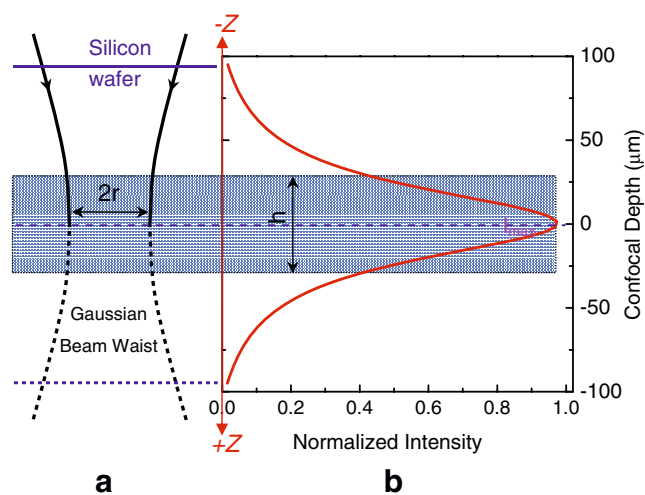


Fig. 2 **a** Waist profile of a laser beam in a solution and **b** the corresponding confocal depth (z) and intensity (I) profile of a moving silicon wafer in an aqueous solution, simulating the collection volume of a solution spectrum

the illuminated volume of the solution can generate Raman signal. The contribution of each molecule becomes less with the increasing deviation from the ideal focal plane due to the lowering of the power density. Meanwhile, the confocal pinhole limits the number of molecules that can be imaged by the CCD detector. These two factors result in the fact that the molecules in the focal plane contribute the most to the overall intensity and the contribution decreases dramatically from the molecules in the plane with increasing distance (z) to the ideally focal plane ($z=0$). In order to estimate the number of molecules contributing to the total signal of solution species, we proposed a method that is to immerse a single-crystal silicon wafer in a solution in the cell with exactly the same setup as that used in surface Raman measurement (including the window and the same thickness of the solution layer, if it is in electrochemical in situ measurement; however, if the surface Raman measurement is done in air, no window or solution layer is necessary). Then, the integrated intensity of the strongest band for Si at 520.6 cm^{-1} was measured while the Si wafer was moved through the illuminated volume and plotted against z (see the solid line in Fig. 2b). This plot is considered the confocal depth profile under the real measuring condition. Experimentally, the solution spectrum is collected from the illuminated volume of the solution and is a sum of signal from all the illuminated plane of the solution, just like the surface of a moving Si wafer, giving the same profile to that of the modeled silicon wafer. It can be seen that the contribution from molecules outside the region of $|z| > 75\text{ }\mu\text{m}$ is negligible to N_{bulk} . Now, assume an ultrathin layer of solution with a thickness of h and volume hA in the vicinity of the ideally focused plane, in which all the molecules have the same contribution to the overall signal as that in the ideal focal plane; the overall signal can be obtained by integrating the signal over the intensity profile. Thus, the thickness h can be calculated by

$$h = \frac{\int_{-\infty}^{\infty} I(z) dz}{I_{\text{max}}} \quad (3)$$

The h value (in micrometers) depends on the pinhole size and the objective lens of the Raman microscope and has been considered the key parameter of a confocal system. It should be especially emphasized that the h value can be significantly different in the case with and without a quartz window and solution layer. For example, the h value will be about $60\text{ }\mu\text{m}$ when the thickness of the solution layer is about $200\text{ }\mu\text{m}$, the thickness of the quartz window is 1 mm , the size of the pinhole is $600\text{ }\mu\text{m}$, and the size of the slit is $200\text{ }\mu\text{m}$, and the objective $\times 50$ is the long working distance one. Whereas, without the quartz window and solution layer, the value is about 15 to $20\text{ }\mu\text{m}$.

The effective illuminated number of molecules in the aqueous solution, N_{bulk} , can be written as

$$N_{\text{bulk}} = AhcN_A \quad (4)$$

where c is the concentration of adsorbate in solution, and N_A the Avogadro constant. From Eqs. (2) and (4), Eq. (1) can be rearranged as

$$G = \frac{cN_A\sigma hI_{\text{surf}}}{RI_{\text{bulk}}} \quad (5)$$

G can be obtained after substituting all the known data and constants into the above equation. The roughness factor R can be estimated by calculating the surface area using simple sphere model for monolayer-dispersed nanoparticles. However, for multilayer nanoparticles or massive electrode surfaces, it is better to use electrochemical methods, such as differential capacitance or cyclic voltammetric methods to estimate the R . σ is generally obtained from literature from previous studies and can also be estimated with known atom size and bond distance; the latter may often lead to an underestimation of σ and therefore the G value. We have shown that the G value of transition metals varies from 1 to 4 orders of magnitude [12, 13, 43–48].

Investigation of benzene adsorption and reaction on transition metal surfaces

The interaction between aromatic compounds and various substrates has been, and continues to be, one of the hot fields in surface sciences since the 1970s [65–74]. Benzene, as the simplest aromatic molecule and with known, clear assignments of all the vibrational modes, has received much attention concerning its reaction and adsorption behavior on metal surfaces. However, it is surprising that different conclusions have been drawn for benzene on different substrates or even the same surface. The ability to obtain SERS from Pt-group metals allows us to investigate the reaction and adsorption behavior of benzene on Pt surfaces. Surprisingly, we found that the seemingly simple system is by no means simple. For example, when the potential is more negative than -0.5 V , a lot of droplets were observed on the Pt surface in $0.1\text{ M KCl} + 9\text{ mM benzene}$ solution. The Raman spectra obtained on these droplets shows the characteristics of cyclohexane, see Fig. 3c, indicating the hydrogenation of benzene in the presence of surface hydrogen on the Pt surface in this potential region. Because cyclohexane is insoluble in aqueous solution, it forms very small droplets preferably on the surface. We did not observe the SERS signal of cyclohexane in a control experiment in solution saturated with cyclohexane, which indicates the observed signal is the normal Raman signal of cyclohexane.

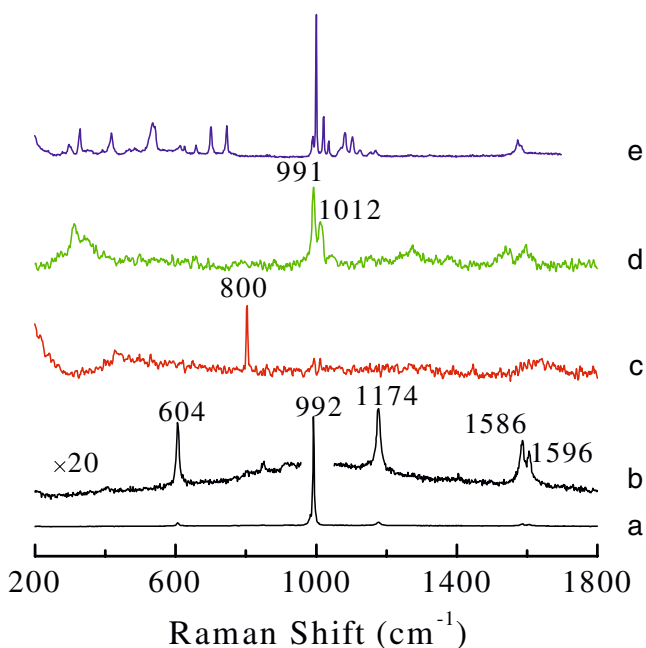


Fig. 3 Normal Raman spectra of liquid benzene (**a** and **b**), and potential-dependent surface Raman spectra on a roughened Pt electrode in 0.1 M KCl solution containing 9 mM benzene at different potentials: **c** -1.0 V, **d** -0.5 V, and **e** 1.4 V. All the Raman measurements in this article were made using 632.8-nm-wavelength emission from a He–Ne laser

Without the spatial resolution provided by the confocal Raman microscope, this observation may not be possible. Surprisingly, this phenomenon was not observed on a smooth Pt surface, indicating the importance of surface roughness, or more specifically, the electrocatalytic activity of the Pt nanoparticles on the roughened Pt surface in the hydrogenation of benzene [75]. The phenomenon points to a promising future of using this reaction to remove benzene from waste water and transforming it into an environmentally benign product.

When the potential was shifted to as positive as 1.2 V, again some tiny dark spots appeared on the Pt electrode. These spots grew into small and evenly distributed transparent drops and adhered to the electrode surface with time or further positive shift of the electrode potential. The Raman spectrum obtained on the droplet shows the characteristics of chlorobenzene with different numbers of substitutions (see Fig. 3e), besides the 992 cm^{-1} band from benzene. We could not obtain the signal in places without droplets indicating the above signal is from the normal Raman signal of chlorobenzene droplet rather than the SERS of chlorobenzene due to the weak interaction between chlorobenzene and the Pt surface. We inferred that the chlorination of benzene occurred in the chloride solution at oxidation potentials on the roughened Pt surface. Because chlorobenzene is insoluble in water, it would form drops adhered to the electrode surface. Such a phenomenon was also observed in the solution containing bromide, but

not in the Γ^- and F^- solution. The different phenomena might be due to the fact that Γ^- can be easily oxidized to I_3^- , whereas F^- is too stable to be oxidized. With moderate electrochemical activity, Cl^- and Br^- can be oxidized on the Pt surface at very positive potentials to form surface radicals, which can then react with benzene adsorbed on the surface to form chlorobenzene or bromobenzene [76].

In the potential region between -0.5 and 0.6 V, very interestingly we observed surface-enhanced Raman signal from the adsorbed benzene [77]. However, the phenomenon was so complicated that it needs more detailed exploration.

Figure 4 shows a set of surface-enhanced Raman spectra from a roughened Pt electrode in a solution containing 9 mM benzene and 0.1 M NaF. At -0.5 V, several Raman peaks at around 991, 1,012, 1,043, 1,271, 1,539, and $1,595\text{ cm}^{-1}$ could be clearly seen in the frequency range from 800 to $1,800\text{ cm}^{-1}$, and are related to that of the benzene vibrations [73, 74]. Meanwhile, two peaks at around 310 and 341 cm^{-1} and a peak at around $3,043\text{ cm}^{-1}$ were observed in the low and high frequency regions, respectively. These peaks show a different relative intensity compared to that of the liquid benzene (see Fig. 3a,b). Their intensities decrease quickly with the positive shift of the electrode potential; however, no obvious Raman shift can be discerned. When the electrode potential was positively shifted to -0.2 V, the analysis of the surface Raman spectra becomes difficult and unreliable due to the laser-induced carbonization of surface adsorbates. At 0.6 V, the signal of the adsorbed benzene vanished due to the oxidation of the platinum surface. It can also be seen from the figure that the bands at 310 and $1,012\text{ cm}^{-1}$ have the same potential

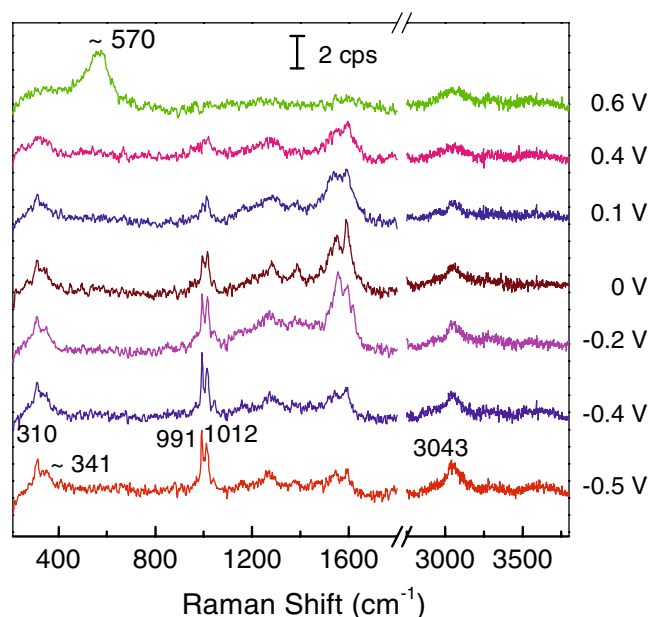


Fig. 4 Potential-dependent surface-enhanced Raman spectra on a roughened Pt surface in 0.1 M NaF solutions containing 9 mM benzene

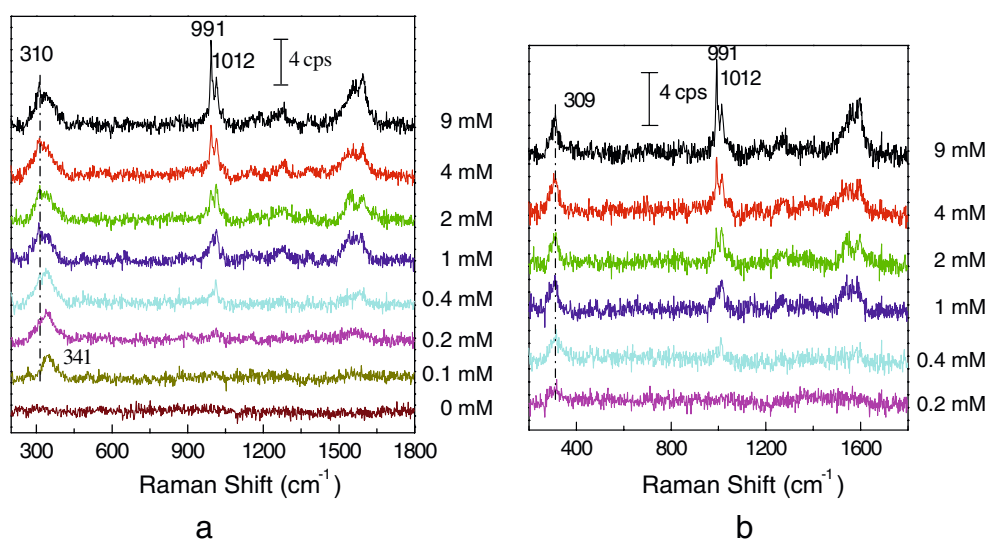
dependence. Meanwhile, the band at 341 cm^{-1} does not change much with potential until the oxidation of the surface. However, on the basis of these data alone, it is still impossible to perceive the adsorption configuration of benzene on Pt. Therefore, we carried out a concentration-dependent Raman study of benzene adsorption and the result is shown in Fig. 5. The solution concentration was changed from 0 to 9 mM (the saturated concentration). All the spectra were acquired at -0.5 V , where the maximum signal of the adsorbed benzene was observed. As can be seen from Fig. 5a, the Raman spectrum is featureless over the frequency range $200\text{--}1,800\text{ cm}^{-1}$ when the solution is free of benzene. At a benzene concentration of about 0.1 mM , a broad band at around 341 cm^{-1} can be clearly seen, and the peak at around $1,012\text{ cm}^{-1}$ is very weak. At a concentration of 0.4 mM , the $1,012\text{ cm}^{-1}$ peak becomes obvious and a weak shoulder at 310 cm^{-1} appears. Meanwhile, the intensity of the peak at 991 cm^{-1} increased steadily with the increasing benzene concentration up to 9 mM .

If we subtract the Raman spectra obtained at 0.1 mM from the spectra obtained at higher benzene concentrations, we can see a clear and narrow peak at ca. 309 cm^{-1} (see Fig. 5b), although no obvious change can be found for other Raman peaks. We can see from the figure that the intensity of the 991 cm^{-1} peak increases almost linearly with the increasing benzene concentration, and meanwhile, the frequency is almost the same as that in solution (992 cm^{-1}). Both facts indicate that this band is from physisorbed benzene that may not directly interact with the metal surface. Therefore, it is reasonable to observe that this peak is very sensitive to the applied potential and can be easily removed from the solid–solution interface with the positive shift of the potential, as shown in Fig. 4. We can clearly find that the 309 and $1,012\text{ cm}^{-1}$ peaks follow

essentially the same trend with concentration, indicating that they may be from the same species. In the literature, it has been found that the ring-breathing mode of benzene (990 cm^{-1}) blue-shifts when one or two of the H atoms are substituted by other functional groups. For example, the band will blue-shift from 992 cm^{-1} (C_6H_6) to $1,008\text{ cm}^{-1}$ ($\text{C}_6\text{H}_5\text{F}$) or even severely blue-shift to $1,053\text{ cm}^{-1}$ ($\text{C}_6\text{H}_4(\text{CH}_3)_2$) [78]. It was found that the weaker the electron-donating ability of the substituent group is, the larger the blue-shift of the ring breathing mode will be. The electronic structure of the Pt atom is $5d^96s^1$ and the Pt atom is normally considered as an electron acceptor. We can then assume that benzene is adsorbed on the Pt surface with one of its hydrogens lost to form $\text{C}_6\text{H}_5\text{Pt}$ and the ring plane perpendicular to the Pt surface, giving Raman bands of the benzene ring breathing mode at $1,012\text{ cm}^{-1}$ and Pt–C band at 309 cm^{-1} . This adsorption configuration makes the ring breathing mode one of the strongest vibrational modes in surface Raman spectra according to the surface Raman selection rule.

It can be seen from Fig. 5a that, at a low benzene concentration, there is only one broad peak at ca. 341 cm^{-1} and we could not detect any other signal accompanying this band. It should be particularly pointed out that the intensity of this band only slightly decreased even after the Pt electrode had been cleaned in $0.5\text{ M H}_2\text{SO}_4$ solution until the recovery of the characteristic cyclic voltammogram after the in situ Raman experiment. This indicates the adsorbed species related to this Pt–C must have a very strong interaction with the Pt surface and is very hard to remove with the electrochemical cleaning process. We may assume that the surface coverage of this species on the Pt electrode is very low because of the negligible effect of this adsorbed species on the cyclic voltammogram of the Pt electrode and the independence of the surface Raman

Fig. 5 **a** Concentration dependence of surface-enhanced Raman spectra on a roughened Pt electrode in 0.1 M NaF solution with benzene concentration indicated in the figure. **b** The corresponding spectra after subtraction of the solution Raman spectrum of 0.1 M NaF containing 0.1 mM benzene



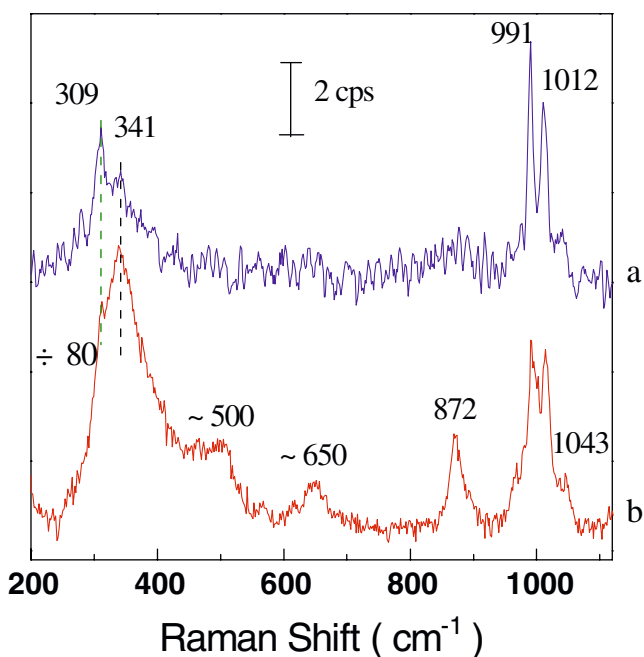


Fig. 6 Surface-enhanced Raman spectra of benzene adsorbed on a roughened Pt (a) and Au@Pt NPs (b) surfaces at -0.5 V in 0.1 M KCl containing 9 mM benzene

intensity of the 341 cm^{-1} peak (Fig. 5a) on the concentration of benzene. To find out the origin of this band, we investigated the adsorption of benzene using a substrate that may provide a higher surface enhancement, i.e., a Au core Pt shell (Au@Pt) nanoparticle assembled electrode, as the SERS substrate [62]. The substrate has the chemical properties of Pt, meanwhile providing high SERS activity boosted by the high electromagnetic field enhancement of the Au core. Figure 6 shows SER spectra of benzene adsorbed on a Au@Pt NPs surface and a roughened Pt surface at -0.5 V in 0.1 M KCl containing 9 mM benzene. The intensity of the former spectrum has been scaled down by a factor of 80 to allow for comparison. Apparently, the spectrum obtained on the Au@Pt substrate shows a much higher signal-to-noise ratio, which allows us to observe the peaks in the frequency region between 400 and 900 cm^{-1} that is too weak to observe on pure Pt surfaces. The bands at around 500 and 650 cm^{-1} could be assigned to the C–C–C out-of-plane bending and C–H out-of-plane bending, respectively [74, 79, 80]. Theoretical calculation has shown that the benzene ring breathing vibration of benzene can vary from 826 to 860 cm^{-1} depending on the adsorption site [78]. Therefore, it is reasonable to assign the band at around 872 cm^{-1} to the benzene ring breathing vibration for benzene parallel-adsorbed on the Pt surface. According to the good correlation in the intensities of the 872 and 341 cm^{-1} bands, we can assign the 341 cm^{-1} band to the Pt–C vibration of this parallel adsorption mode. In the two Pt–C bands detected, the band related to the parallel mode has a higher frequency as compared with the vertical one,

indicating that the parallel-adsorbed benzene has a stronger interaction with the Pt substrate owing to a better electron cloud overlap between the π electrons of the benzene ring and the d orbitals of the Pt atom. If we compared Fig. 6b with Fig. 6a and Fig. 5, we will find that the relative intensity of the flatly adsorbed benzene to that of vertically dissociated adsorbed benzene is different, which can be understood from the different surface structure of the platinum surface prepared using different methods. This assumption is supported by the fact that the flatly adsorbed benzene has a stronger interaction with the (100) facet, whereas dissociated-adsorbed benzene can only be found on the (110) facet [77, 81].

We have also investigated the adsorption behavior on Ru, Rh, and Pd surfaces. On Pd, Rh, and Ru surfaces, the parallel-chemisorbed species are the dominant surface species, with a decreasing amount of physisorbed species [77]. Even for the parallel-chemisorbed species, the red-shift of the ring breathing vibration decreases in the order of Pt, Ru, Rh, and Pd, which can be explained by the different d orbital electronic structures of the four metals [82]. It should be pointed out that although the study was carried out on rough surfaces, the distinct effect of metal on the adsorption behavior of benzene on different metal surfaces can still be found and the main result is still consistent with that obtained on single-crystal surfaces.

Effect of co-adsorbed species on the adsorption behavior of benzene on Rh

Besides the effect of the substrates, considerable efforts have been devoted to study the co-adsorption of benzene with other species for a better understanding of benzene adsorption behavior on various surfaces. Indeed, we have found very interesting co-adsorption behavior of benzene with other adsorbates on Rh [81].

Figure 7 gives the potential-dependent surface Raman spectra on a roughened Rh electrode in 0.1 M KCl containing 9 mM benzene with and without pyridine. All peaks within the shaded areas are from the adsorbed pyridine. After the addition of pyridine, both the position and the intensity of the Raman peaks of the adsorbed benzene change slightly and the potential-dependence behavior of benzene adsorption is almost the same as that free of pyridine [77], which indicates pyridine has little effect on benzene adsorption on Rh. However, we did observe a minor negative shift in the potential for the hydrogenation of benzene to cyclohexane after the addition of pyridine, which is evident by the sharp peak at 800 cm^{-1} (marked with double plus) from cyclohexane. Furthermore, the potential-dependent adsorption behavior of pyridine on the Rh surface is almost the same as that free of benzene

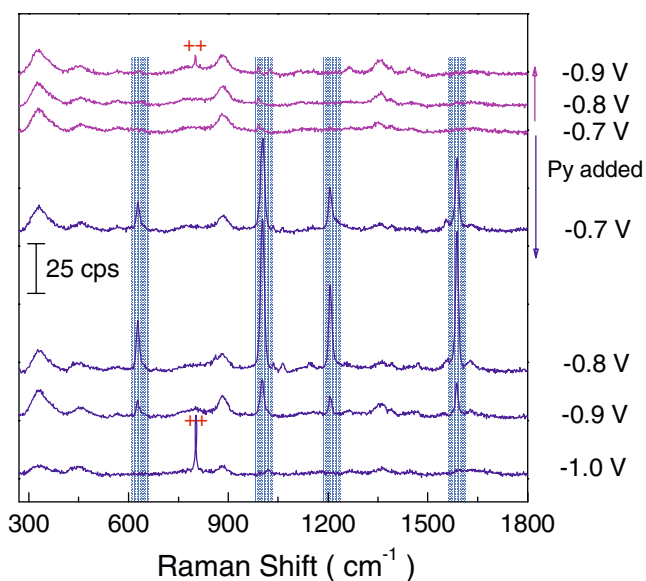


Fig. 7 Potential-dependent surface-enhanced Raman spectra on a roughened Rh surface in 0.1 M KCl containing 9 mM benzene with (blue) or without (magenta) 0.1 mM pyridine. Pyridine was added with potential controlled at -0.7 V. Peaks within shaded areas are from adsorbed pyridine

(not shown), considering both the intensities and frequencies of surface Raman peaks of pyridine [48]. The above results indicate that both the adsorption behavior of pyridine and benzene will not be influenced by the existence of the other species, from which we can postulate that under the present conditions, benzene and pyridine

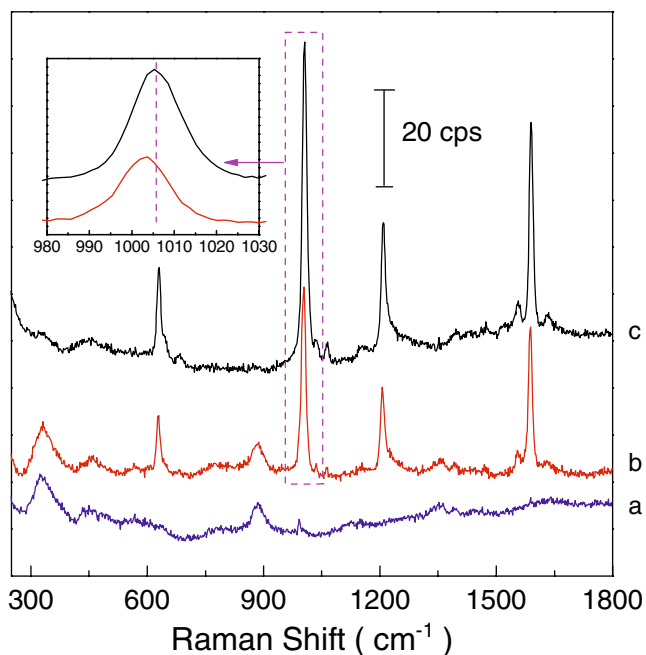


Fig. 8 Surface-enhanced Raman spectra on a roughened Rh surface in 0.1 M KCl at -0.7 V: **a** containing only 9 mM benzene, **b** containing 9 mM benzene and 1 mM pyridine, **c** containing only 1 mM pyridine. The insert is an expanded view of spectra **b** and **c**

tend to adsorb on different sites on the roughened Rh surface and the interaction between pyridine and benzene is very weak. The hindrance of the hydrogenation of benzene after the addition of pyridine indicates that pyridine prefers to occupy the surface sites where hydrogen ions used to adsorb.

When the concentration of pyridine is increased to 1 mM, the position and intensity of surface Raman peaks of the adsorbed benzene still remain unchanged, see Fig. 8. However, the surface Raman intensity of pyridine is only half that of the case free of benzene. Furthermore, the peak position of ring breathing vibration of pyridine red-shifts from $1,005$ to $1,003$ cm^{-1} at -0.7 V due to the existence of benzene. With the increase of the bulk pyridine concentration and therefore the interfacial pyridine concentration, the surface coverage should increase accordingly until a saturated adsorption is achieved. However, under the present conditions, the strong interaction between the benzene molecules and the Rh surface makes it difficult for pyridine to displace the adsorbed benzene or to occupy some suitable adsorption sites due to the steric effect from surrounding adsorbed benzene. Both factors hinder the maximum adsorption of pyridine at this concentration.

In the case of SCN^- , when 1 mM NaSCN was added into 0.1 M KCl solution containing 9 mM benzene at -0.5 V, no signal from benzene could be detected, indicating that benzene molecules were totally repelled from the Rh surface, as shown in Fig. 9. The same potential dependence of surface Raman spectra of SCN^- and the

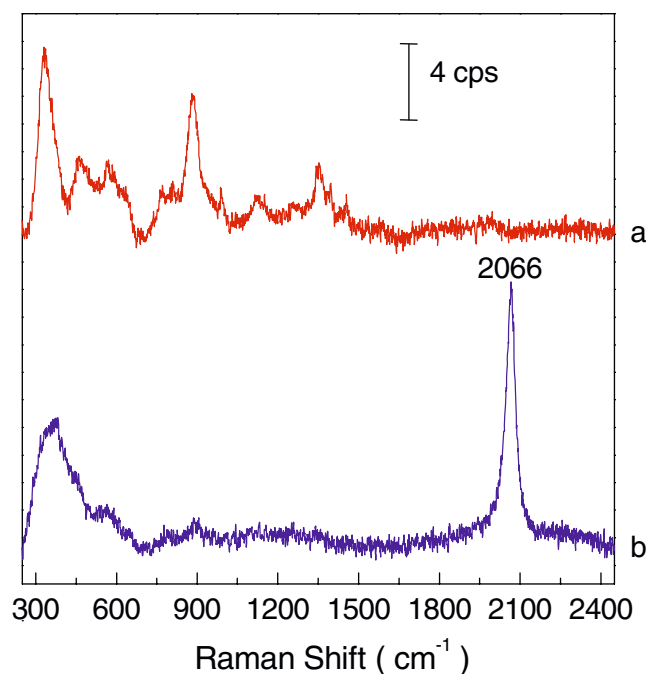


Fig. 9 Surface-enhanced Raman spectra on a roughened Rh electrode in 0.1 M KCl containing **a** 9 mM benzene and **b** 9 mM benzene and 1 mM NaSCN. The potential was -0.7 V

same C–N vibration position at each potential studied as that free of benzene (not shown) indicate a negligible effect of benzene in the interfacial region on the adsorption of SCN^- on the Rh surface. We also found that the adsorption of SCN^- is too strong to be removed from the Rh surface through a conventional electrochemical cleaning process, indicating that SCN^- is the strongest adsorbate among the three species on the roughened Rh surface.

SERS mechanism in transition metal systems

The SERS mechanism is always an important issue in the SERS field and has attracted much interest from various communities of surface science, spectroscopy, condensed-phase physics, and nanoscience. On the basis of our experimental results correlated with surface roughness at the nanometer scale, we strongly believe the existence of the EM enhancement. Meanwhile, the excitation-wavelength dependence of the intensity–potential profile observed in some SERS systems gives strong evidence that the chemical enhancement is operative as well in these systems.

Electromagnetic enhancement mechanism

The electromagnetic field enhancement of the Ag, Au, and Cu is considered to mainly come from geometrically defined surface plasmon resonances (SPRs) at metal nanostructures [15, 16, 83–86]. The surface Raman enhancement arising from the SPR of a spherical nanoparticle can be estimated using the following equation:

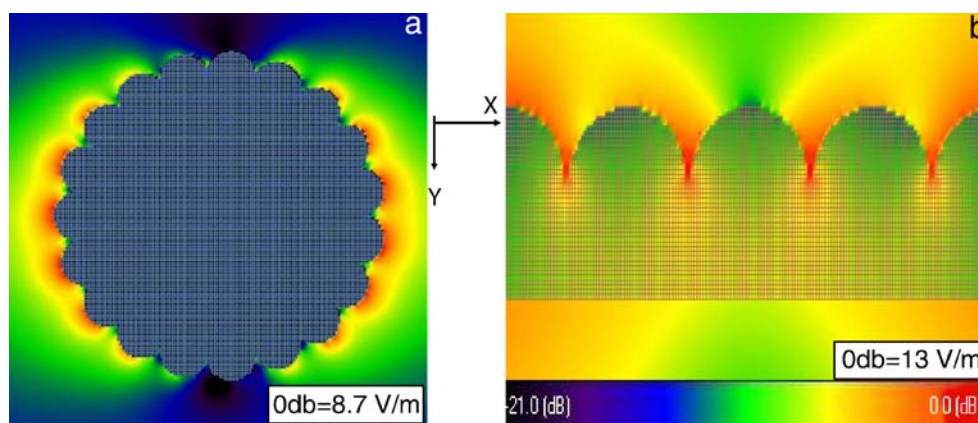
$$G(\omega) \propto \left| \frac{\varepsilon_i - \varepsilon_0}{\varepsilon_i + 2\varepsilon_0} \right|^2 \cdot \left| \frac{\varepsilon_s - \varepsilon_0}{\varepsilon_i + 2\varepsilon_0} \right|^2 \cdot \left(\frac{r}{r+d} \right)^{12} \quad (6)$$

where ε_0 is the dielectric constant of the medium, ε_i is the wavelength-dependent complex dielectric constant of the metal nanoparticles, r is the radius of the nanoparticles, and d is the distance of the point to be measured to the center of the nanoparticle. Considering that in most of SERS studies the medium is water and $\varepsilon_0=1.77$, when the real part of ε_i approaches -3.54 and the imaginary part approaches 0, the enhancement reaches the maximum. Some free electron metals, such as Ag, Au, and Cu, can meet this condition and therefore produce very high enhancement. When the shape of the nanoparticles deviates from the spherical nanoparticles, such as ellipsoids or rods, the lightning-rod effect should be considered due to the existence of the high curvature points. Furthermore, more and more experimental and theoretical studies demonstrate that the coupling between nanoparticles can effectively increase the enhancement effect. These general conclusions can also be borrowed to analyze the case of transition metal systems.

In comparison with coinage metals, transition metals have very different electronic structures, where the Fermi level locates at the d band and the interband excitation occurs very possibly in the visible light region [87, 88]. The coupling between conduction electrons and interband electronic transitions in the transition metal systems will considerably lower the quality of their surface plasmon resonances [55, 56]. In fact, most transition metals show a large imaginary part of the dielectric constants and therefore are not effective in generating high SERS activity over the visible light region. Indeed, except Pd, we did not find obvious wavelength-dependent behavior of transition metals in the visible light region [49]. However, it has been found that the electromagnetic field near the high-curvature points on the rough surface, i.e., the lightning-rod effect, can result in the largest electric field near the sharpest surface of the needle-like rod [85]. As a consequence, the maximum enhancement has been found at the spheroid tip and the field strength increases with the aspect ratio [19]. Accordingly, the lightning-rod effect may play a more important role in the EM enhancement for transition metals. Besides, it has also been found that the coupling between nanoparticles is also very important in transition metal system.

In order to simulate the enhancement in transition metal systems, we did a very preliminary estimation of the enhancement effect. We have found that several surfaces with a cauliflower-like morphology can exhibit a high SERS activity [47, 48]. To explain these experimental observations, the electric-field enhancement of SERS-active Rh systems was estimated by using the 3D-FDTD method [63]. Two types of models were used to simulate the cauliflower-like nanoparticles: a Rh sphere with a diameter of 120 nm covered with 20-nm semispherical particles, and a flat Rh surface decorated with nanohemispheres of 20 nm, as shown in Fig. 10. The calculated electric-field distribution on the surface is visualized in color. It can be seen that the magnitude of the maximally enhanced electric field on the cauliflower nanoparticle is about 8–9 times higher than that of the incident light, and the highest enhancement usually appears at the apex of small hemispheres in the “cauliflower” (Fig. 10a). It corresponds to a ca. 6×10^3 -fold SERS enhancement on these sites. Note that the magnitude of the maximum electric-field enhancement is just about 4-fold compared with that of the incident light for the smooth sphere under the same excitation conditions, which means that the maximal enhancement factor for the cauliflower-like nanoparticle is just about 17 times larger than that for the smooth sphere. This different field enhancement could probably be understood on the basis of the lightning-rod effect, which usually results in a relatively large electric-field enhancement near high-curvature sites on the surface [83]. This is contrary to the maximal field enhancement at

Fig. 10 FDTD simulated electric-field distribution for a cauliflower-like Rh nanoparticle (a) and a flat Rh surface decorated with small nanohemispheres (b). The laser beam illuminates along the y -direction with x -polarization. The scale bar is given at the bottom of (b)



the junction point of two nanoparticles. However, if the cauliflower is detached and extended into a plane grating-like structure, the field maximum is shifted to the crevices, as shown in Fig. 10b. The symmetric nature of the nanoparticle may play a role in limiting the electromagnetic modes when the nanostructure is coupled with an incident plane wave [89]. Our results seem to indicate that the EM enhancement is very sensitive not only to the wavelength and polarization of the exciting light, the electronic properties of the metal, and the surface morphology, but also to the symmetric nature of the SERS nanostructures.

Chemical enhancement

Chemical enhancement, according to its definition, includes any enhancement of the Raman intensity of surface species resulting from its chemical interaction with surface or other surface species and is clearly correlated to the charge transfer between the probed molecule and surface or other surface species. One should note the following three types of charge-transfer process contribute to the chemical enhancement [90]: (1) when a molecule interacts with the surface or other surface species, the electron distribution and therefore the polarizability of molecule will change. Such a change may cause different enhancements for different vibrational modes; (2) metal ion, probed molecule, and electrolyte ion may form a surface complex, leading to the change of the polarizability of the molecule. Some surface complexes may even create a new electronic level in resonance with the incident laser energy, similar to the resonance Raman effect of a complex; (3) the third type is the most complicated one and called photon-driven charge-transfer process or often simplified as charge transfer. This process occurs when the incident laser energy matches the energy difference between the surface molecules' HOMO or LUMO and Fermi level or surface state of the metal substrate. This process could also be associated with the excited state of the whole molecule/metal system and with the charge transfer between the molecule and the metal

surface (or surface ad-clusters). It could result in a considerable increase in the Raman intensity of probe molecules. The photon-driven charge-transfer mechanism has been used to explain the change of intensity–potential profile with the changing excitation line and is the most important type of chemical enhancement mechanism.

We observed clearly the type I and III charge-transfer processes. Taking pyridine, a model molecule widely used in SERS, and different adsorbed transition metals as an example, we can observe a dramatic change of the relative intensity of the two main SERS bands assigned to the total symmetric a_1 modes at ca. $1,008\text{ cm}^{-1}$ and $1,035\text{ cm}^{-1}$, respectively (see Fig. 11) [13]. This behavior cannot be explained well by the EM mechanism. On the other hand, using a hybrid density functional theory study of the binding interaction and the Raman spectral properties of pyridine–metal clusters, we demonstrated that the bonding

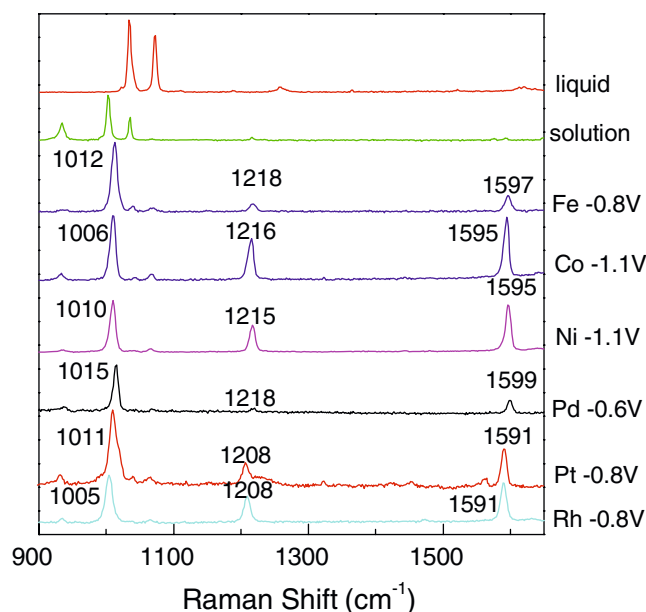


Fig. 11 Raman spectra of pure liquid pyridine and pyridine solution, and surface-enhanced Raman spectra of pyridine adsorbed on transition-metal surfaces at potentials with maximum intensity

interaction influences the relative Raman intensity of the vibrational modes significantly, resulting in the metal-dependent SERS spectra [91]. Therefore, we need to keep in mind that when the molecule adsorbs on the metal surface, the change in the electron distribution of molecule even under its electronic ground state may cause different enhancements for different vibrational modes.

Besides such an effect, we also observed a photon-driven charge-transfer process on many transition metal surfaces, including Pt and Co [64, 92]. Actually, the photon-driven charge-transfer mechanism can be easily verified by obtaining the intensity–potential profile with the changing excitation line.

Taking the ring breathing vibrational mode of the pyridine adsorbed on Co, for example, when all the experimental conditions were kept the same and the excitation line was changed from 514.5 nm to 632.8 nm, the potential of the maximal SERS intensity was negatively shifted by 130 mV [92]. In comparison, the potential shift is about 200 mV for Pt [64]. We have found that the contribution of chemical enhancement to the total SERS is ca. 1 order of magnitude for the adsorbed pyridine on the Co electrode, whereas the contribution of EM enhancement is about 2 orders of magnitude.

It should be noted that many molecules and ions are adsorbed much more strongly at the transition metal surfaces than that at the noble metal systems. When the strong chemical bond is formed, this chemisorption not only changes the electronic structure of adsorbate itself but also influences to some extent the surface electronic structure. This may cause a frequency shift of the surface plasmon resonances and lead to a change of the local electric field at the metal surface. Quantum mechanical schemes, describing the SERS enhancement based on the surface plasmon polariton model involving the interaction of the surface with the light, have been suggested by several groups [93–95]. It was proposed that the total process is a sequence consisting of the creation of the surface plasmon excitation [96, 97], its inelastic scattering, and finally its annihilation by the radiating photons. More recently, a quantum chemical scheme has been performed to calculate the surface enhancement factor and to analyze the shape and size effect of nanoparticles adsorbed by molecules [98–100]. Hopefully, this study can be further extended to the transition metals soon with the aid of more powerful computational methods.

Conclusion and outlook

This review intends to provide an overview of the SERS on transition metals. In order to obtain the weak SERS signal from transition metal surfaces, it is not only very important

to make a good design of the optical configuration, but also important to obtain a substrate with the highest possible enhancement effect. A method for estimating the surface enhancement effect in the confocal system was introduced to obtain reliable surface enhancement. Based on this consideration, we have been able to extend the SERS study to the reaction and adsorption of benzene on Pt surfaces. With the information provided both in the low frequency region of metal and adsorbate bonding and the high frequency region of the internal molecular vibrations, we found that benzene can be hydrogenated to cyclohexane on the Pt surface in the negative potential region, while it is halogenated in the positive potential region. In between these two regions, three types of benzene adsorption modes have been observed: the physisorbed benzene, the chemisorbed benzene with one or two of the hydrogens on the benzene ring dissociated, and the parallel-chemisorbed benzene with the ring parallel to the metal surface. This observation highlights the unique advantage of Raman spectroscopy over other vibrational spectroscopy methods in getting the full range of vibrational information under electrochemical conditions, which is very useful for understanding the surface and interfacial processes.

Although great progress has been made in Raman spectroscopy on transition metals, we should note that there are still some hurdles to the wider application of Raman spectroscopy in transition metal systems. Fortunately, some new opportunities have recently appeared. Accordingly, we will briefly describe some possible developments in the Raman spectroscopy on transition metals in terms of the SERS substrate and these emerging techniques.

SERS substrates

Ordered nanostructured surfaces

How to obtain a SERS substrate with very uniform structure and highest possible enhancement is a key issue of SERS and for quantitative application. Although electron [101, 102] and focused ion [103] beam lithography or SPM (STM and AFM) lithography [104, 105] can produce ideally ordered periodic arrays with optimized particle size, shape, and interparticle spacing, the relatively low efficiency associated with these point-by-point approaches make the fabrication process very slow. Nanostructured surfaces with a large area can be prepared more easily and quickly by the template synthesis technique, especially when combined with the self-assembly method and sphere lithography. The promising templates include the polystyrene and silica spheres or anodic aluminum oxide template [106–108]. Various materials can be filled controllably into a designed template of two- or three-dimensional ordered

nanopores (holes or channels). The template is then removed, leaving behind the spheroid, rod, or wire array with the desired aspect ratio. By controlling the filling time, the interparticle spacing can be adjusted to some extent. Progress in fabricating these two-dimensional nanostructured surfaces will provide great opportunity for not only optimizing the SERS activity of existing materials but also searching for a new class of SERS-active materials, such as bimetals, alloys, and sandwiched materials.

Nanostructured single-crystal surfaces

Ever since the early days of SERS, there have been attempts to directly obtain surface Raman signals from well-defined single-crystal surfaces, since this would be very helpful for studying the orientation of adsorbates unambiguously, for comparing surface selection rules of conventional Raman spectroscopy and SERS, and for getting mechanistic information about surface processes. However, Raman studies on single-crystal surfaces have been extremely difficult because of insufficient intensity due to the absence of or only minor levels of SERS enhancement for smooth surfaces. Very few investigations have been reported in this field and these were performed in a vacuum, an electrochemical environment, or a special attenuated total reflection (ATR) cell [109–111]. The situation may change significantly owing to advances in the two fields. One is related to the rapid development of nanotechnology, which allows the synthesis of nanoparticles with single-crystal structures. Such nanoparticles, on the one hand, can have exposed single-crystal surface, and on the other hand, due to the size is on the scale of several tens of nanometers, can produce SERS enhancement [54–56, 63, 89, 112–114]. If one can assemble these nanocrystals into a very ordered structure with controlled inter-particle spacing, one may be able to obtain SERS from these single-crystal nanoparticles and may be able to bridge the gap between single-crystal surfaces of fundamental interest and highly rough surfaces of practical importance and then eventually link surface science and nanoscience. The second approach is the development of tip-enhanced Raman spectroscopy (TERS). TERS can provide external enhancement to the single-crystal surfaces of noble metals or transition metals [115, 116], which will be introduced later.

Core-shell nanoparticles as SERS substrates

Although transition metals themselves can provide moderate surface-enhanced Raman effect, sufficient for detecting some surface species with moderate Raman cross-section, in general the Raman measuring time for such experiments takes about 30 to 200 s, which is not suitable for studying the surface dynamics. Furthermore, for some species with

very low Raman cross-section, it is still difficult to obtain signals with reasonable good signal-to-noise ratio, or the signal is still below the detection limit.

To solve this problem, probably the best way is still to use the borrowing SERS strategy. To exclude the pinhole problem and the trivial processes in obtaining the thin layer substrate, recently, our group has been able to obtain core-shell nanoparticles, with Au nanoparticles with varying diameter as the core, and different transition metals as the shell, using a two-step seed method in nearly epitaxial growth mode for Pd and Pt [62, 63]. When the thickness of the shell is only about five atomic layers, the core-shell nanoparticles can still have the electromagnetic enhancement effect from the Au core and the chemical properties of the transition metal shell, which can provide much higher enhancement as compared with pure transition metal substrates or nanoparticles. By dispersing the core-shell nanoparticles over an electrode surfaces, e.g., glassy carbon, silicon, or other material electrodes, we can use them for in situ electrochemical measurement. With the high enhancement, we have been able to obtain SERS signals of adsorbed CO, hydrogen, and even water. Indeed, we have found very different behavior for water on Au, Pt, Pd, and Rh surfaces [117]. This result points to the promising future of using core-shell nanoparticles for investigating the dynamic process or even the intermediates during electrochemical reactions.

Tip-enhanced Raman spectroscopy

Recently, a new approach has been developed to enhance the Raman scattering intensity, by combining Raman microscop-

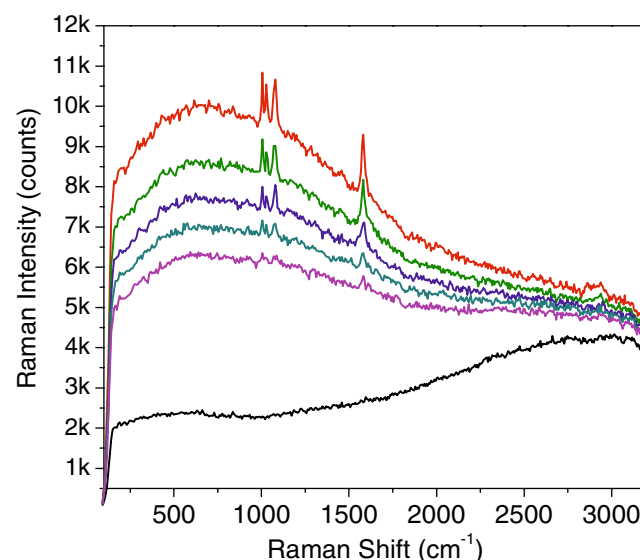


Fig. 12 Tip-enhanced Raman spectra for benzenethiols at Pt (110). *Bottom curve* is for the tip-retracted case; the *upper curves* are for the tip-tunneling case

py with scanning probe microscopy. By illuminating the gap (with width of 1 to several nm) of a gold or silver SPM tip and the substrate with a laser of suitable wavelength and polarization, localized surface plasmons can be excited inside the gap, producing a large increase of the electromagnetic field and resulting in a significant increase of the Raman intensity in a region having the size of the tip apex. This approach is known as TERS [118–120], which has the advantage of the high spatial resolution of SPM and the rich chemical information of Raman spectroscopy and can be applicable to metal–vacuum, metal–gas phase, or metal–electrolyte interfaces. Since the enhancement is restricted to the tip–substrate gap, the enhancement can be created on flat transition metal surfaces.

Using this technique, surface Raman signals from non-resonant adsorbate (benzenethiol) on Pt single-crystal surfaces have been obtained [115], and the results are shown in Fig. 12. For example, on Pt(110) surface, in the absence of the tip, no Raman signal can be detected. However, when the Au tip is moved into the tunneling position above the Pt (110) substrate, high-quality spectra can be obtained. Although it takes 60 s to acquire a spectrum with a sufficiently high signal-to-noise ratio, the recording of a Raman spectrum of optically nonresonant species adsorbed at a smooth Pt(110) surface represents a breakthrough in the field of surface Raman spectroscopy. This example illustrates that the detection of species adsorbed in (sub)monolayer quantities on smooth single-crystal metal surfaces is no longer a difficult task, even if the adsorbates exhibit moderate or weak Raman cross sections.

For adsorbates on single-crystal surfaces, additional information (such as molecular orientation) can be achieved by choosing appropriate light polarization in TERS and analyzing the response with respect to surface selection rules. With the high spatial resolution of TERS applied to the study of probe molecules having a high sensitivity to the binding site, it might become possible to reveal the role of terraces, steps, and different facets during the adsorption process or in the course of chemical reactions in catalytic and electrochemical processes. Additionally, TERS may provide clues to the nature of SERS-active sites. Recently TERS has been used for characterizing the membrane structure of cells as well as the structures of carbon nanotubes [121, 122]. We are optimistic that TERS will be developed as a valuable analytical tool, providing simultaneous spectroscopic and microscopic information in the nanometer region, which ultimately may include single-molecule detection and investigation.

In situ SERS study

By taking advantage of advances in the Raman instrumentation and the fast development of different types of

transition metal substrates with a high enhancement, it is now feasible to study the process occurring or intermediates produced under real catalytic or electrocatalytic conditions, including at solid–gas, solid–liquid, and solid–liquid–gas three-phase interfaces, with strict control of the temperature, gas pressure, and electrode potential [123].

Acknowledgements The present work is supported by the Natural Science Foundation of China (20473067, 20673086, 20433040, 20021002, 20228020), Ministry of Education of China (20040384010, NCET-05-0564) and Fok Ying Tung Foundation (101015).

References

1. Fleischmann M, Hendra PJ, McQuillan AJ (1974) *Chem Phys Lett* 26:163–166
2. Jeanmaire DL, Van Duyne RP (1977) *J Electroanal Chem* 84:1–20
3. Albrecht MG, Creighton JA (1978) *J Am Chem Soc* 99:5215–5216
4. Aroca RF (2006) *Surface-enhanced vibrational spectroscopy*. Wiley, Berlin
5. Cotton TM (1988) *Adv Spectrosc* 16:91–153
6. Garrell RL (1989) *Anal Chem* 61:401A–411A
7. Pemberton JE (1991) In: Abruna HD (ed) *Electrochemical interfaces: modern technique for in-situ interface characterization*. VCH, Berlin, pp 193–263
8. Birke RL, Lu T, Lombardi JR (1991) In: Varma R, Selman JR (eds) *Techniques for characterization of electrodes and electrochemical processes*. Wiley, New York, pp 211–277
9. Pettinger B (1992) In: Lipkowski J, Ross PN (eds) *Adsorption at electrode surface*. VCH, New York, pp 285–345
10. Campion A, Kambhampati P (1998) *Chem Soc Rev* 27:241–250
11. Kneipp K, Kneipp H, Itzkan I, Dasari RR, Feld MS (1999) *Chem Rev* 99:2957–2975
12. Tian ZQ, Ren B, Wu DY (2002) *J Phys Chem B* 106:9463–9483
13. Tian ZQ, Ren B (2004) *Annu Rev Phys Chem* 55:197–229
14. Baker GA, Moore DS (2005) *Anal Bioanal Chem* 382:1751–1769
15. Moskovits M (1985) *Rev Mod Phys* 57:783–826
16. Kerker M (1984) *Acc Chem Res* 17:271–277
17. Otto A, Mrozek I, Grabhorn H, Akemann W (1992) *J Phys Condens Matter* 4:1143–1212
18. Lombardi JR, Birke RL, Lu TH, Xu J (1986) *J Chem Phys* 84:4174–4180
19. Cline MP, Barber PW, Chang RK (1986) *J Opt Soc Am B* 3:15–21
20. Van Duyne RP, Haushalter JP (1983) *J Phys Chem* 87: 2999–3003
21. Oblonsky LJ, Devine TM, Ager JW, Perry SS, Mao XL, Russo RE (1994) *J Electrochem Soc* 141:3312–3317
22. Fleischmann M, Tian ZQ (1987) *J Electroanal Chem* 217:385–395
23. Fleischmann M, Tian ZQ, Li LJ (1987) *J Electroanal Chem* 217:397–410
24. Aramaki K, Ohi M, Uehara J (1992) *J Electrochem Soc* 139:1525–1529
25. Leung LWH, Weaver MJ (1987) *J Electroanal Chem* 217:367–384
26. Leung LWH, Weaver MJ (1987) *J Am Chem Soc* 109:5113–5119

27. Zou S, Weaver MJ (1998) *Anal Chem* 70:2387–2395
28. Zou S, Weaver MJ, Li XQ, Ren B, Tian ZQ (1999) *J Phys Chem B* 103:4218–4222
29. Weaver MJ, Zou S, Chan HYH (2000) *Anal Chem* 72:38A–47A
30. Park S, Yang P, Corredor P, Weaver MJ (2002) *J Am Chem Soc* 124:2428–2429
31. Zou SZ, Weaver MJ (1999) *J Phys Chem B* 103:2323–2326
32. Cooney RP, Fleischmann M, Hendra PJ (1977) *J Chem Soc Chem Commun* 235–237
33. Pettinger B, Tiedemann U (1987) *J Electroanal Chem* 228:219–228
34. Pettinger B, Friedrich A, Tiedemann U (1990) *J Electroanal Chem* 280:49–59
35. Bryant MA, Loa SL, Pemberton JE (1992) *Langmuir* 8:753–756
36. Taylor CE, Pemberton JE, Goodman GG, Schoenfish MH (1999) *Appl Spectrosc* 53:1212–1221
37. Maeda T, Sasaki Y, Horie C, Osawa M (1993) *J Electron Spectrosc Relat Phenom* 64/65:381–389
38. Bilmes SA, Rubim JC, Otto A, Arvia AJ (1989) *Chem Phys Lett* 159:89–96
39. Bilmes SA (1990) *Chem Phys Lett* 171:141–146
40. Shannon C, Campion A (1988) *J Phys Chem* 92:1385–1387
41. Yamada H, Yamamoto Y (1981) *Chem Phys Lett* 77:520–522
42. Yamada H, Yamamoto Y (1983) *Surf Sci* 134:71–90
43. Tian ZQ, Ren B (2003) In: Bard AJ, Stratmann M, Unwin PR (eds) *Encyclopedia of electrochemistry*. Wiley-VCH, Weinheim, pp 572–659
44. Tian ZQ, Ren B, Mao BW (1997) *J Phys Chem B* 101:1338–1346
45. Huang QJ, Yao JL, Gu RA, Tian ZQ (1997) *Chem Phys Lett* 271:101–106
46. Cao PG, Yao JL, Ren B, Mao BW, Gu RA, Tian ZQ (2000) *Chem Phys Lett* 316:1–5
47. Wu DY, Xie Y, Ren B, Yan JW, Mao BW, Tian ZQ (2001) *Phys Chem Comm* 18:1–3
48. Ren B, Lin XF, Yan JW, Mao BW, Tian ZQ (2003) *J Phys Chem B* 107:899–902
49. Liu Z, Yang ZL, Cui L, Ren B, Tian ZQ (2007) *J Phys Chem C* 111:1170–1175
50. Guo L, Huang QJ, Li XY, Yang SH (2001) *Phys Chem Chem Phys* 3:1661–1665
51. Gómez R, Pérez JM, Solla-Gullón J, Montiel V, Aldaz A (2004) *J Phys Chem B* 108:9943–9949
52. Gómez R, Solla-Gullón J, Pérez JM, Aldaz A (2005) *ChemPhysChem* 6:2017–2021
53. Gómez R, Solla-Gullón J, Pérez JM, Aldaz A (2005) *J Raman Spectrosc* 36:613–622
54. Zettsu N, McLellan JM, Wiley B, Yin YD, Li ZY, Xia YN (2005) *Angew Chem Int Ed* 45:1288–1292
55. Xiong YJ, McLellan JM, Chen JY, Yin YD, Li ZY, Xia YN (2005) *J Am Chem Soc* 127:17118–17127
56. McLellan JM, Xiong YJ, Hu M, Xia YN (2006) *Chem Phys Lett* 417:230–234
57. Kim NH, Kim K (2004) *Chem Phys Lett* 393:478–482
58. Kim NH, Kim K (2005) *J Raman Spectrosc* 36:623–628
59. Ren B, Lin XF, Jiang YX, Cao PG, Xie Y, Huang QJ, Tian ZQ (2003) *Appl Spectrosc* 57:419–427
60. Gu W, Ren B, Gu RA, Tian ZQ (2007) (in preparation)
61. Zuo C, Jagodzinski PW (2005) *J Phys Chem B* 109:1788–1793
62. Li JF, Yang ZL, Ren B, Liu GK, Fang PP, Jiang YX, Wu DY, Tian ZQ (2006) *Langmuir* 22:10372–10379
63. Tian ZQ, Yang ZL, Ren B, Li JF, Zhang Y, Lin XF, Hu JW, Wu DY (2006) *Faraday Discuss* 132:159–170
64. Cai WB, Ren B, Li XQ, She CX, Liu FM, Cai XW, Tian ZQ (1998) *Surf Sci* 406:9–22
65. Steinruck HP, Huber W, Pache T, Menzel D (1989) *Surf Sci* 218:293–316
66. Somorjai CA (1994) *Introduction to surface chemistry and catalysis*. Wiley, New York
67. Lehwald S, Ibach H, Demuth JE (1978) *Surf Sci* 78:577–590
68. Haq S, King DA (1996) *J Phys Chem* 100:16957–16965
69. Lin RF, Koestner RJ, Van Hove MA, Somorjai GA (1983) *Surf Sci* 134:161–183
70. Neumann M, Mack JU, Bertel E, Netzer FP (1985) *Surf Sci* 155:629–638
71. Koel BE, Crowell JE, Mate CM, Somorjai GA (1984) *J Phys Chem* 88:1988–1996
72. Mate CM, Somorjai GA (1985) *Surf Sci* 160:542–560
73. Zou SZ, Williams CT, Chen EKY, Weaver MJ (1998) *J Am Chem Soc* 120:3811–3812
74. Zou SZ, Williams CT, Chen EKY, Weaver MJ (1998) *J Phys Chem B* 102:9039–9049
75. Liu GK, Yao JL, Ren B, Gu RA, Tian ZQ (2002) *Electrochem Commun* 4:392–396
76. Liu GK, Ren B, Gu RA, Tian ZQ (2002) *Chem Phys Lett* 364:593–598
77. Liu GK, Ren B, Wu DY, Duan S, Li JF, Yao JL, Gu RA, Tian ZQ (2006) *J Phys Chem B* 110:17498–17506
78. Bernhard S (1989) *Raman/Infrared atlas of organic compounds*. VCH, Weinheim
79. Morin C, Simon D, Sautet P (2004) *J Phys Chem B* 108:5653–5665
80. Varsanyi G (1974) *Assignments for vibrational spectra of seven hundred benzene derivatives*. Wiley, New York
81. Liu GK, Ren B, Gu RA, Tian ZQ (2007) *J Phys Chem C* 111 (in press)
82. Brewer L (1969) *Science* 161:115–122
83. Gersten J, Nitzan A (1980) *J Chem Phys* 73:3023–3037
84. Adrian FJ (1981) *Chem Phys Lett* 78:45–49
85. Metiu H (1984) *Prog Surf Sci* 17:153–320
86. Schatz GC, Young MA, Van Duyne RP (2006) *Top Appl Phys* 103:19–46
87. Weaver JH (1975) *Phys Rev B* 11:1416–1425
88. Ordal MA, Bell RJ, Alexander RW Jr, Long LL, Querry MR (1985) *Appl Opt* 24:4493–4499
89. Tian ZQ, Yang ZL, Ren B, Wu DY (2006) *Top Appl Phys* 103:125–147
90. Tian ZQ (2006) *Faraday Discuss* 132:156–157
91. Wu DY, Duan S, Ren B, Tian ZQ (2005) *J Raman Spectrosc* 36:533–540
92. Xie Y, Wu DY, Liu GK, Huang ZF, Ren B, Yan JW, Yang ZL, Tian ZQ (2003) *J Electroanal Chem* 554:417–425
93. Malinsky MD, Kelly KL, Schatz GC, Van Duyne RP (2001) *J Am Chem Soc* 123:1471–1482
94. Kim CW, Villagran JC, Even U, Thompson JC (1991) *J Chem Phys* 94:3974–3977
95. Persson BNJ (1993) *Surf Sci* 281:153–162
96. Otto A (1984) In: Cardona M, Guntherodt G (eds) *Light scattering in solid*. Springer, Berlin, vol 4, pp 289–418
97. Pettinger B (1986) *J Chem Phys* 85:7442–7451
98. Corni S, Tomasi J (2001) *Chem Phys Lett* 342:135–140
99. Corni S, Tomasi J (2001) *J Chem Phys* 114:3739–3751
100. Corni S, Tomasi J (2002) *J Chem Phys* 116:1156–1164
101. Felidj N, Aubard J, Levi G, Krenn JR, Salerno M, Schider G, Lamprecht B, Leitner A, Aussenegg FR (2002) *Phys Rev B* 65:075419.1–075419.9
102. Gunnarsson L, Bjerneld EJ, Xu H, Petronis S, Kasemo B, Kall M (2001) *Appl Phys Lett* 78:802–804
103. Brolo AG, Arcetander E, Gordon R, Leathem B, Kavanah KL (2004) *Nano Lett* 4:2015–2018
104. Kolb DM, Ullmann R, Will T (1997) *Science* 275:1097–1099
105. Piner RD, Zhu J, Xu F, Hong SH, Mirkin CA (1999) *Science* 283:661–663

106. Zhang X, Whitney AV, Zhao J, Hicks EM, Van Duyne RP (2006) *J Nanosci Nanotech* 6:1920–1934
107. Abdelsalam ME, Bartlett PN, Baumberg JJ, Cintra S, Kelf TA, Russellet AE (2005) *Electrochem Comm* 7:740–744
108. Yao JL, Pan GP, Xue KH, Wu DY, Ren B, Sun DM, Tang J, Xu X, Tian ZQ (2000) *Pure Appl Chem* 72:221–226
109. Perry SS, Hatch SR, Champion A (1996) *J Chem Phys* 104:6856–6859
110. Sakamoto K, Hashizume H, Nagafusa M, Sato H, Ushioda S (1996) *Surf Sci* 368:292–295
111. Bruckbauer A, Otto A (1998) *J Raman Spectrosc* 29:665–672
112. Sun YG, Xia YN (2002) *Science* 298:2176–2179
113. Ahmadi TS, Wang ZL, Green TC, Henglein A, El-Sayed MA (1996) *Science* 272:1924–1926
114. Sau TK, Murphy CJ (2004) *J Am Chem Soc* 126:8648–8649
115. Pettinger B, Ren B, Picardi G, Schuster R, Ertl G (2004) *Phys Rev Lett* 92:096101
116. Ren B, Picardi G, Pettinger B, Schuster R, Ertl G (2005) *Angew Chem Int Ed* 44:139–142
117. Jiang YX, Li JF, Wu DY, Ren B, Yang ZL, Hu JW, Chow YL, Tian ZQ (2007) (submitted)
118. Verma P, Inouye Y, Kawata S (2006) *Top Appl Phys* 103:241–262
119. Pettinger B (2006) *Top Appl Phys* 103:217–242
120. Bouhelier A (2006) *Microsc Res Tech* 69:563–579
121. Neugebauer U, Rösch P, Schmitt M, Popp J, Julien C, Rasmussen A, Budich C, Deckert V (2006) *Chemphyschem* 7:1428–1430
122. Anderson N, Hartschuh A, Cronin S, Novotny L (2005) *J Am Chem Soc* 127:2533–2537
123. Ren B, Cui L, Lin XF, Tian ZQ (2003) *Chem Phys Lett* 376:130–135